computation

MDPI

Article

Chelating Mechanisms of Transition Metals by Bacterial Metallophores "Pseudopaline and Staphylopine": A Quantum Chemical Assessment

Ghassan Ghssein [1] and Samir F. Matar [2,*,†]

[1] Lebanese German University, Tyre 1601, Lebanon; g.ghssein@lgu.edu.lb
[2] Lebanese German University, Sahel-Alma Campus, P.O. Box 206, Jounieh, Lebanon
* Correspondence: s.matar@lgu.edu.lb or abouliess@gmail.com
† Formerly at CNRS, ICMCB, University of Bordeaux, 351 cours de la Libération, 33400 Talence, France.

Received: 6 September 2018; Accepted: 24 October 2018; Published: 31 October 2018

Abstract: In bacterial pathology, metallophores fabricated by bacteria such as *Staphylococcus aureus* and *Pseudomonas aeruginosa* are exported to surrounding physiological media via a specific process to sequester and import metals, resulting in enhanced virulence of the bacteria. While these mechanisms are understood at qualitative levels, our investigation presents a complementary original view based on quantum chemical computations. Further understanding of the active centers in particular was provided for pseudopaline and staphylopine metallophores, which were described chemically and with vibration spectroscopy. Then, for complexes formed with a range of transition metal divalent ions (Ni, Cu, and Zn), description and analyses of the frontier molecular orbitals (FMOs) are provided, highlighting a mechanism of metal-to-ligand charge transfer (MLCT), based on excited-states calculations (time-dependent density functional theory (TD-DFT)) at the basis of the delivery of the metallic ionic species to the bacterial medium, leading eventually to its enhanced virulence. Such investigation gains importance especially in view of stepwise syntheses of metallophores in the laboratory, providing significant progress in the understanding of mechanisms underlying the enhancement of bacterial pathologies.

Keywords: chelators; drugs; bacteria; quantum molecular chemistry; frontier molecular orbitals; vibration spectroscopy

1. Introduction and General Context

Chelation (pronounce "kelation" as it comes from Greek, meaning "pliers") is a chemical process through which a complex is formed between a metallic ion and a chemical molecule (ligand) through ionic and coordination bonding. It is an important mechanism, as it involves research and application fields of food science, bioscience, biochemistry, bacteriology, and therapy. Regarding the latter, chelation therapy consists of the patient's intake of specific drugs (such as ethylenediaminetetraacetic acid (EDTA)) which bind to toxic metals such as heavy metals (lead, mercury, arsenic, etc.) present in the organism. Once the metal is chelated (bonded) to the active center of the drug, the body removes the produced complex through urination and discharge of feces [1].

A significantly important case is the excess of iron overdose incurred through intensive blood transfusions and in the thalassemia major disease encountered in the Mediterranean population [2]. Here, specific chemical chelators (siderophores) trap free ferrous and ferric ions to eliminate them. Among others, a recognized drug in this context is 4-(3,5-bis(2-hydroxyphenyl)-1,2,4-triazol-1-yl)benzoic acid, commercially known as deferasirox [2]. Figure 1a shows a representation of the molecule. The chelating centers created upon removal of the two hydroxyl hydrogens are shown with green lines. Here and

in the following case studies, the ridding of H from the OH hydroxyl centers prior to chelation with divalent transition ions (TM^{++}) in the physiologic medium is poorly understood.

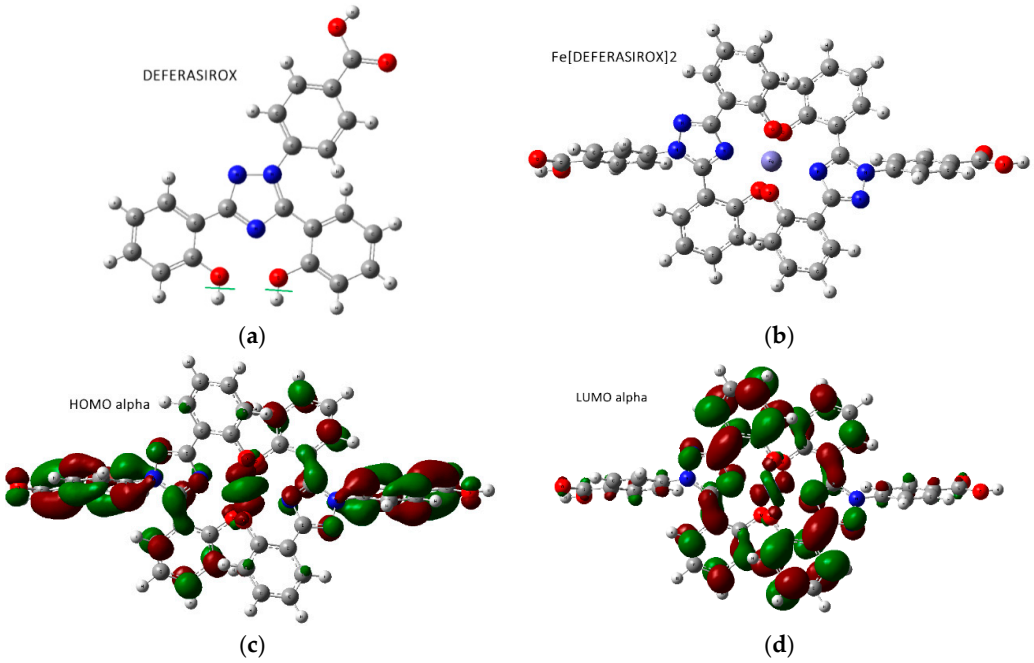

Figure 1. Deferasirox as an iron chelator for therapeutic applications. (**a**) Single molecule with the chelating centers created by removing two hydroxyl H as shown with green lines; (**b**) two molecules needed to chelate the iron(III) ion (Fe^{3+}) within an octahedral coordination; (**c**,**d**) frontier molecular orbitals (FMOs)—highest occupied molecular orbitals (HOMOs) and lowest unoccupied molecular orbitals (LUMOs)—obtained with quantum chemical calculations at the 6-31g/UB3LYP level (U stands for unrestricted needed when a paramagnetic ion such as Fe^{3+} $3d^5$ -or Cu^{2+} $3d^9$ hereafter- is involved; cf. text). $\Delta E(HOMO - LUMO) \approx 0.26$ eV.

It actually takes two molecules to chelate a central iron, forming a distorted octahedron around it with four planar oxygen ions and two axial nitrogen atoms (Figure 1b). Understanding the interaction of Fe with its chemical surrounding calls for analysis of the molecular orbitals (MOs), especially the frontier ones. MO analyses obtained from geometrically unconstrained molecular calculations at the quantum level (cf. Section 2) lead to the examination of the highest occupied molecular orbitals (HOMOs; Figure 1c). The overlap of lobes of the Fe *d* orbital recognized with d_z^2 symmetry can be observed with the *p*-O orbitals and less so with N, with which weaker coordination bonds are expected (i.e., not ionic-like as with O^-); the remaining charge density is distributed over the benzoic COOH regions of the two deferasirox ligands. In the lowest unoccupied molecular orbitals (LUMOs; Figure 1d), there is a redistribution of electrons over the other regions of the ligand molecule not involved in the HOMOs. Moreover, iron is clearly much less bonded, as exhibited by the nearly free d_z^2 lobes. A thorough quantum chemical study of deferasirox and its chelation with different TM is underway, especially in the context of further properties related to chemotherapy.

The context presented above readily introduces the main topic of the present paper, regarding bacterial pathology. In all bacteria, transition metals are considered as essential micronutrients; therefore, their acquisition is vital, especially in metal-scarce conditions, such as in a bacterial host. Consequently, pathogenic bacteria developed many different mechanisms for their uptake and homeostasis [3]. Indeed, through a particular process called nutritional immunity framework, the host tends to sequester metals, and the pathogen, in order to keep up with its metal requirements, increases its metal uptake efforts [4]. To accomplish this mission, most pathogenic bacteria produce small

molecules dedicated to metal uptake, called metallophores. The most well-characterized metallophore family is that of siderophores (sider = iron) [5].

Metallophore molecules are synthesized within the cytoplasm and then exported to the extracellular medium, where they scavenge iron. Extracellular iron–siderophore complexes can be recognized and actively transported into the periplasm by TonB-dependent transporters (TBDT) in Gram-negative bacteria, and are usually transported across the plasma membrane by ATP-binding cassette (ABC) transporters in both Gram-negative and Gram-positive bacteria [6]. This metallophore is also considered as a virulence factor in some bacteria, such as pyochelin and pyoverdine in *Pseudomonas aeruginosa* [7]. Other metallophores were also described in the literature for their ability to uptake metals other than iron, such as chalcophore for copper [8,9], manganesophore for manganese [10], nickelophore for nickel [11–13], and zincophore for zinc [14–16]. Recent studies showed two new metallophores, related to the nicotianamine of plants, in *Staphylococcus aureus* and *Pseudomonas aeruginosa,* called staphylopine (STP) and pseudopaline (PSP), respectively [17,18]. STP is known as a broad-spectrum metallophore for its ability to chelate different transition metals (TMs) [17], and PSP is known as a narrow-spectrum metallophore, because it is more specific for the chelation of nickel and zinc [18].

The exportation of the metallophore outside the bacterial membrane and its subsequent uptake of the chelated complex both underlie in vivo mechanisms which are hard to measure (e.g., for obtaining infrared (IR), Raman, and ultraviolet–visible (UV–Vis) spectra constituting spectroscopic signatures). However, in 2017, Zhang et al. [19] reported the stepwise total syntheses of natural metallophores (staphylopine and aspergillomaramine). This new direction can permit further quantitative spectroscopic characterization for better understanding the underlying mechanisms. Nevertheless, substantial input pertaining to getting vibration signatures, as well as the characterization of the frontier molecular orbitals FMO, highlighting chemical center activities can be obtained at the quantum chemistry level with ab initio calculations. Specifically, frontier orbitals involving electron exchange between the metal and the metallophore point to specific regions of the so-formed complex chemical system, and they describe energetic zones involved with the chemical bonding and its changes. Calling for frontier orbitals to interpret reaction mechanisms is based on the FMO theory devised by Fukui in mid-20th century [20].

The mechanism of chelation within metallophores, outside the bacteria, whereby active centers of the molecule interact with the metal, is not well understood, and our purpose here was to present original results of a quantum molecular study of PSP and STP molecules and their interactions with the first series of divalent TM ions, i.e., 3*d* diamagnetic ions, such as Ni^{2+} and Zn^{2+}, with the narrow-spectrum metallophore, PSP, and the broader-spectrum STP. Paramagnetic Cu^{2+} and diamagnetic Ni^{2+} and Zn^{2+} were used in FMO analyses and assessments of IR spectra in a physiological medium outside the bacterial cell.

2. Frameworks of Theory and Computations

In quantum chemistry calculations [21], it is well established that calling for a density functional theory (DFT) [22,23] framework brings accurate results regarding the energy (E)-dependent quantities and E-derived properties. This is because the exchange and correlation (XC) effects are equally treated, albeit at a "local level", i.e., at the location of the electron, which then becomes a "quasi-particle". In this context, far from nuclear physics, the quasi-particle is defined as the electron surrounded by an impenetrable space called "the exchange–correlation hole", which consists of merging the Fermi hole (exchange) and the Coulomb hole (correlation). Note that exchange is better accounted for in Hartree–Fock (HF) than in DFT because it is done non-locally. The approximation of XC is usually accounted for locally with the local density approximation (LDA) [24], and the gradient of XC is determined using the generalized gradient approximation (GGA) [25]. Taking the best of the HF and DFT solutions led to improvements in ab initio molecular calculations with so-called "hybrid functionals", consisting of mixing exact exchange following HF- and DFT-based correlation. The most accurate results are found using hybrid functional B3LYP [26] basis sets coupled with all electrons,

such as the Pople 6-31g split-valence basis set [27]. Results presented herein were obtained using this hybrid functional/basis set framework. Multiprocessor calculations, massively parallelized, were done using the Gaussian 09 code [28] (see acknowledgements). Furthermore, in order to account for the physiological medium, we used the polarizable continuum model (PCM) [29] implemented within Gaussian 09. The PCM model is based on a self-consistent solution of the quantum mechanical problem of a molecule immersed in such a polarizable medium (water in this study). Following fully unconstrained geometry optimization, one gets a minimum energy. This step is followed by the computation of the vibration frequencies. These are obtained from the energy second derivatives with respect to the lattice coordinates, before being transformed into mass-weighted coordinates.

Furthermore, to better understand the process involved with the FMOs, an accurate description of electronic excitations is required. This can be provided using time-dependent DFT (TD-DFT) calculations, leading to the identification of natural transition orbitals (NTO) [30] which describe hole–particle transitions. Such (heavy) calculations were used in this study for two specific cases of Zn^{2+} complexes with both metallophores under inspection.

3. Results and Discussions

3.1. Molecular Study of Both Metallophores: Pseudopaline and Staphylopine

The molecular structures of PSP and STP were graphically constructed on computer, capturing their spatial three-dimensional (3D) representation with respect to the various carbon hybridizations: tetrahedral sp^3 involving ~109° H–C–H angles and planar sp^2 with 120° angles (Figure 2). This preliminary step was followed by full geometry relaxation using the 6-31g/B3LYP hybrid functional basis set. The resulting geometries are shown in Figure 2. PSP and STP show resemblance on the basis of the chemical groups characterizing them, particularly with the presence of a terminal imidazole ring (on the left-hand side) and several carboxylic groups (COOH)—four in PSP and three in STP. These groups are mediated by aliphatic C–N–C chains. The quantum chemical calculations allowed the extraction of the molecular orbitals, especially the frontier ones (i.e., HOMO and LUMO), as well as the vibrational spectroscopy signatures (IR spectra). The FMO's s show the concentrations of electron density in specific molecular regions, thus pointing to the (re)active zones of the molecules, based on the relationship between chemical reactions and FMOs. Specifically, they involve the right-hand side containing COOH . . . (NH) . . . COOH moieties. This is somewhat close to the deferasirox molecular chelating center of OH . . . N(triazol) . . . OH (Figure 1d).

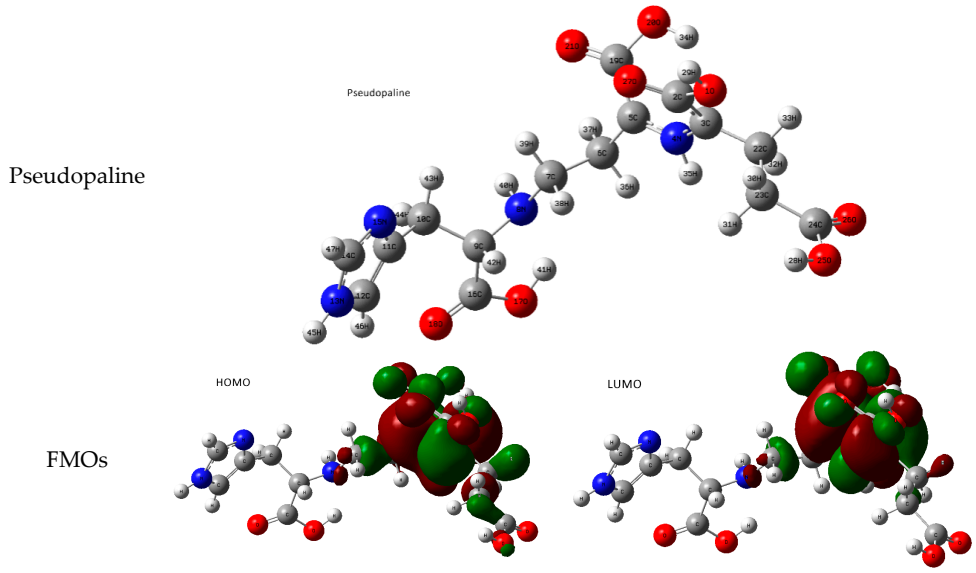

Figure 2. *Cont.*

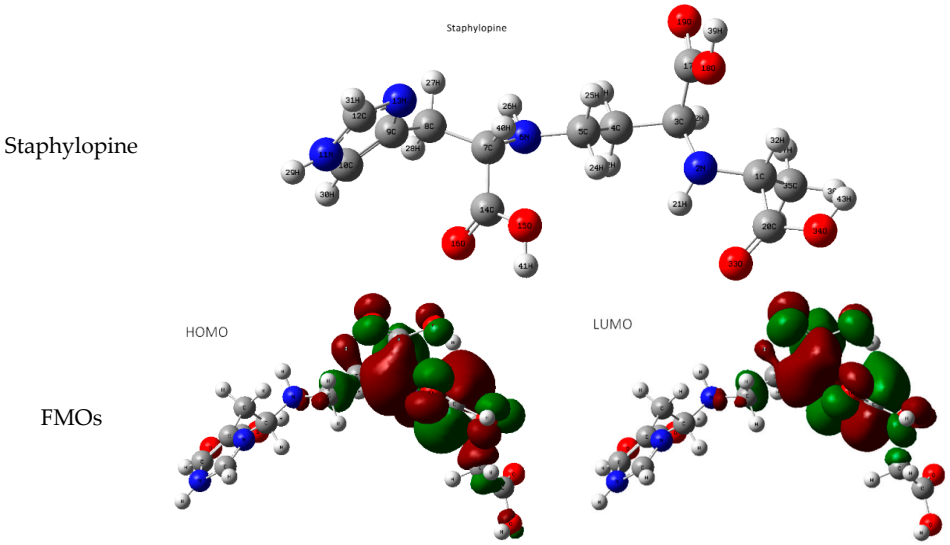

Figure 2. The molecules of both metallophores under consideration—pseudopaline and staphylopine—and their FMOs, highlighting the active centers. Chelating centers were created upon removing two hydroxyl H. Notice the resemblance with the deferasirox active chelating center (Figure 1a). The numbering of some C and O atoms were used in Table 1 to assign vibrations.

Table 1. Main infrared (IR) frequencies in pseudopaline and staphylopine obtained from the B3LYP/6-31g quantum molecular calculations. The numbering of some C and O atoms is as shown in Figure 2.

Designation	Infrared Wave Number (cm^{-1})	
	Pseudopaline	**Staphylopine**
Whole molecule	9.27	11.62
Stretching all molecule	170.71	157.03
Imidazole torsion	649.81	643.43
COOH stretching torsion	773.97	745.85
Imidazol in-plane distortion	954.73	962.07
C–C stretching	1035.72	1057.10
C–N–C stretching	1125.66	1144.20
C–O–H angular torsion	1216.88	1196.49
CH_2/NH dangling	1325, . . . , 1515	1315, . . . , 1556
C=O stretching	1718.45: 19C–21 & 2C–27OO	1705.68: 17C–19O
	1776.65: 16C–18O	1726.27: 14C–16O
	1783.79: 24C–26O	1751.66: 20C–33O
C–H stretching	3027, . . . , 3225	2953–3525
N–H stretching	3225, . . . , 3439	3525, ..., 3566
O–H stretching	3548, . . . , 3633	3587, . . . , 3635
Imidazol–H stretch	3680.12	3672.13

3.1.1. IR Spectra

The calculated spectra for the two molecules in the geometrically relaxed structure are given in Figure 3. The attributions of the main bending, torsion, and stretching modes are given in Table 1. As a general trend, at low frequencies (low wave numbers in cm^{-1}), the whole molecule undergoes bending and torsion, with modes of individual chemical groups appearing most reactive at high frequencies corresponding to O–H, N–H, and C–H stretching.

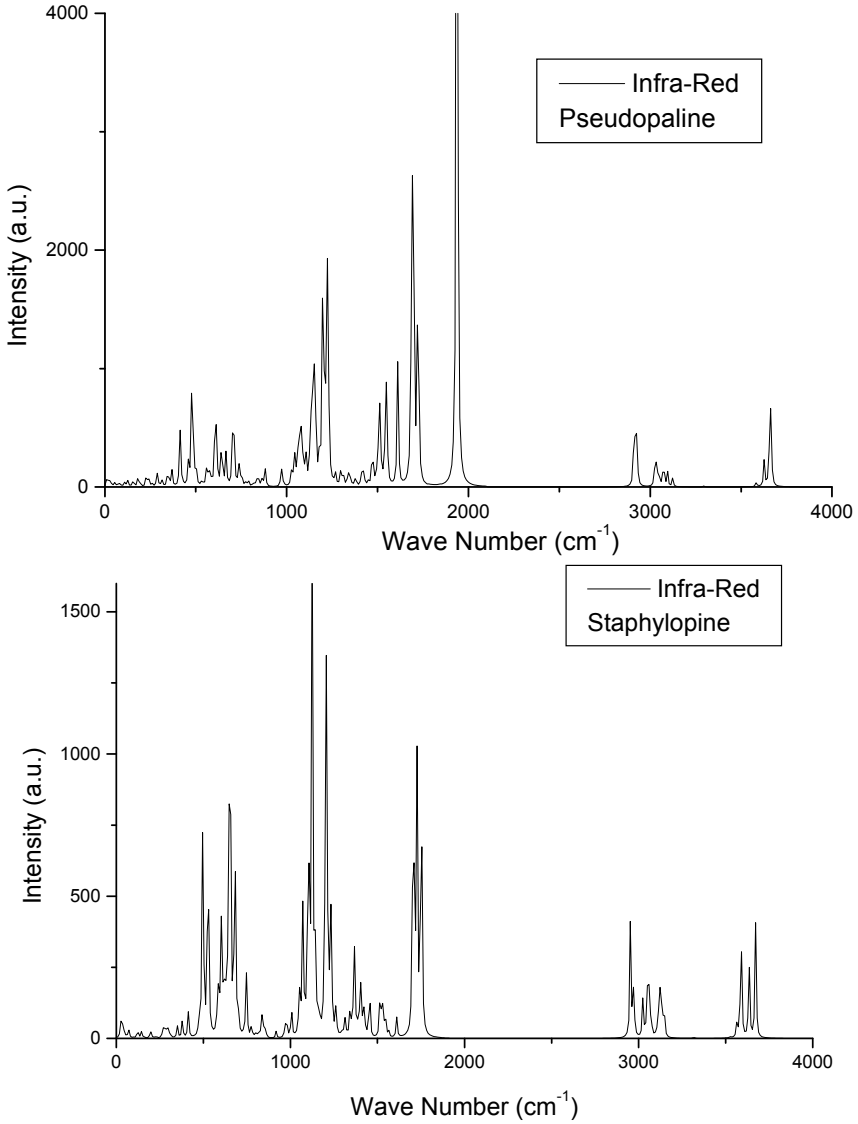

Figure 3. Infrared spectra of pseudopaline and staphylopine. Attributions are provided in Table 1.

3.1.2. Geometry of the Complex

The step following the study of the metallophore consisted of creating chelating centers. This was done by removing the two hydroxyl hydrogen atoms numbered in Figure 2 as 34H and 29H in PSP, and 43H and 39H in STP. The resulting anionic molecule was negatively charged (2^-), enabling it to be neutralized upon receiving a cationic metal charged 2^+, as shown in Figure 4 with Mg^{2+} as an example, along with actually chelated transition metal cations (Ni^{2+}, Cu^{2+}, and Zn^{2+}). Note that these cations are frequently found in a planar coordination, i.e., opposite to Fe^{2+}, which is mainly found in an octahedral environment (cf. Reference [31] and works cited therein). Lastly, regarding the chelating sites, a resemblance with the deferasirox single-molecule active chelating center can be observed (Figure 1a). This geometry of the complex is applied in the external region of the bacteria. In fact, Song et al. [32] determined the crystal structures of CntA/STP/metal for a series of transition-metal cations within a bacterial host, i.e., where the complex was detected by the bacterial receptor CntA. In these conditions, a pseudo octahedral-like environment was evidenced. Nevertheless, there is no crystallographic structure describing the actual geometry of the complex outside a bacterial cell, i.e., in the physiological medium where chelation occurs. Trials with computer construction were attempted by enforcing a folding of the metallophore molecule into an octahedral-like environment around the metal. This construction was then submitted to full geometry relaxations. The result was a total

unfolding/reopening of the molecule, as shown herein. Through intensive exchange with the referees, it can be proposed that the size of the ion is not enough to be completely chelated; thus, depending on their size and nature, ions may or may not stabilize the octahedral environment. Future systematic studies of transition metals with these metallophore ligands should enable further assessments.

3.2. Chelating Metal Ions Using Pseudopaline and Staphylopine

3.2.1. Attempts of Chelation with Alkaline Earth Mg^{2+}

The specificity of metallophores toward transition metals called for an assessment of this feature toward a non-transition element, whereby the magnesium divalent ion Mg^{2+} was used as an example. Full geometry relaxation calculations were carried out with PSP and STP. Hydroxyl H atoms were removed from both molecules and they were allowed to uptake Mg^{2+}, resulting in charge-neutral complexes. The FMOs are shown in Figure 4. Clearly, the molecular region surrounding Mg is devoid of any electron density. This confirms that no chemical interactions took place with an alkaline earth non-transition element, whether in the HOMO or in the LUMO. The only changes occurred in the ligand–ligand charge redistribution within the molecule.

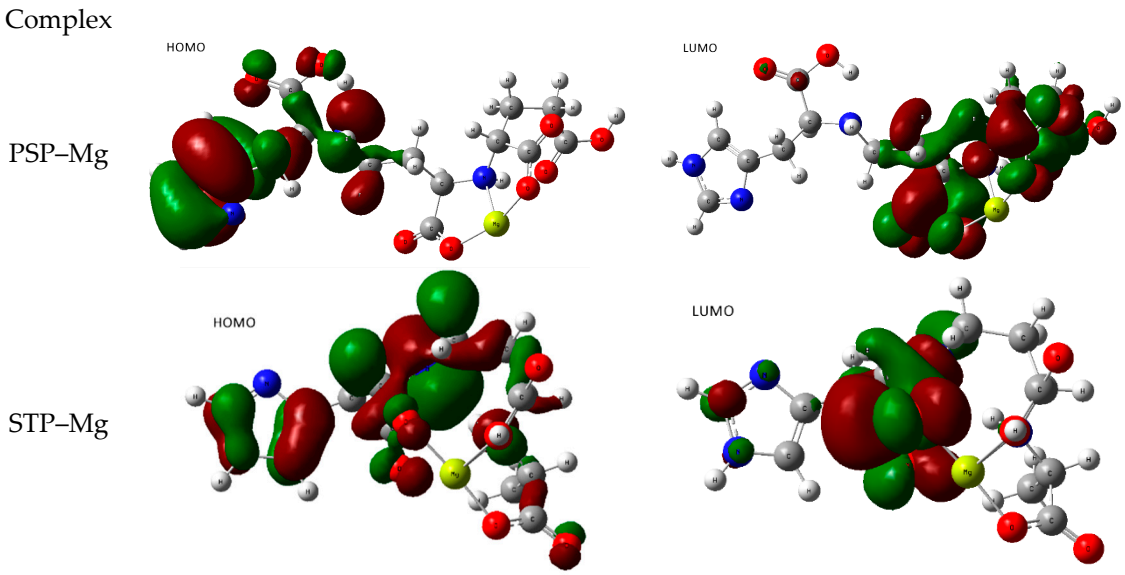

Figure 4. FMOs of pseudopaline (PSP) and staphylopine (STP) complexes with the alkaline earth Mg ion as an example. Indeed, the respective Mg regions show no MOs around the ion, thus highlighting the specificity of such metallophores toward transition-metal ions.

3.2.2. Chelation with Transition-Metal Ions (TM^{++})

Pseudopaline with Divalent Ni and Zn

Figure 5 provides the FMO's. In the case of the PSP–Zn complex, the HOMOs show a large charge density around the metallic ion. Upon exciting the LUMO (energy in the range of 0.6 eV), charge density is transferred to the ligand surrounding the metallic ion. The PSP–Ni complex shows electron concentration in the same region surrounding Ni; however, the mechanism of transfer was different from the zinc case: the *d* orbitals in the HOMO had a d_{x2-y2} characteristic, while a highly intense green non-bonding lobe was observed for the LUMO, pointing to an unstable ligand–metal complex. The energy difference (HOMO − LUMO) was lowered to 0.25 eV.

Further assessment of the FMOs can be accessed through a description of the electronic excitations involved. This can be provided through time-dependent DFT (TD-DFT) calculations. TD-DFT calculations for the geometry optimized molecular structure (ground-state molecular structure) led to

the identification of natural transition orbitals (NTO), through an account for particle (occupied initial state)/hole (formerly unoccupied final state) states. The NTOs corresponding to FMO transition are shown for PSP–Zn in Figure 6. The left-hand side (NTO particle) is in good agreement with Figure 5 for the HOMO, and the right-hand side figure shows the transfer of charge density to the ligand, also in agreement with Figure 5; however, the imidazol region (also observed in the LUMO of the Ni complex in Figure 5) is implicated. Nevertheless, the results of the excited-state calculations show the trend of metal-to-ligand charge transfer (MLCT).

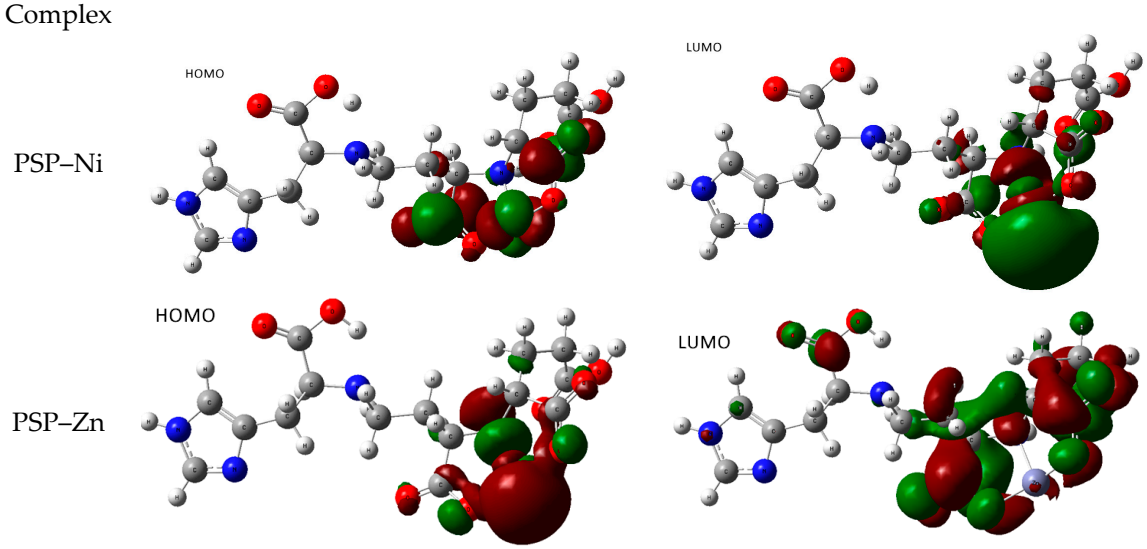

Figure 5. HOMOs and LUMOs of complexes of pseudopaline with divalent Ni and Zn.

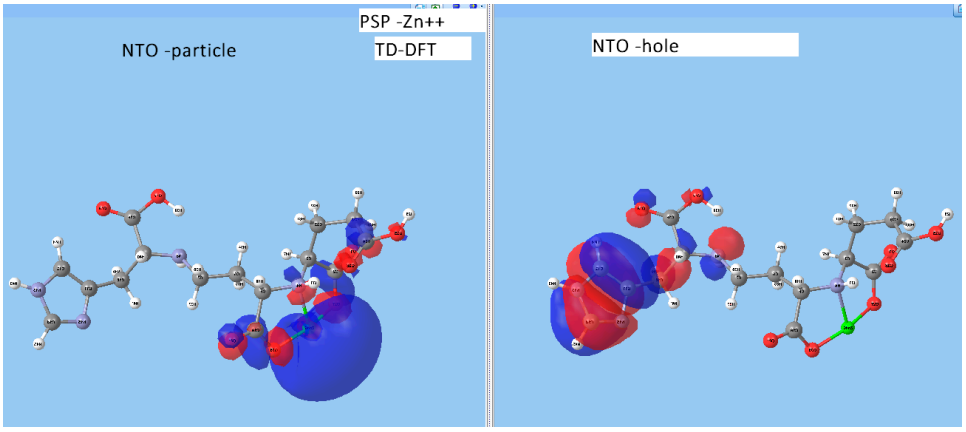

Figure 6. Natural transition (molecular) orbitals (NTOs) corresponding to FMOs of PSP–Zn.

Staphylopine with Divalent Ni, Cu, and Zn

The frontier orbitals are shown in Figure 7. The HOMO of the nickel complex shows similarities with the PSP complex above, with the d_{x2-y2} characteristic revealing a planar-like coordination. However, the transition to the LUMO designates an MLCT-type mechanism (see Figure 8), showing a largely reduced charge density around Ni and a redistribution of electrons over the ligands, including the imidazole ring. The energy difference (HOMO − LUMO) was ~0.38 eV.

The copper complex shows a typical HOMO-to-LUMO MLCT characteristics, concomitant with the highest affinity for such TMs observed experimentally [17]. This is demonstrated by the large electron density around Cu^{2+} (HOMO) and the distribution of electron density over the ligands in LUMO, while Cu^{2+} is surrounded by hardly any charge density. The energy change (HOMO − LUMO) was lowered to ~0.23 eV. This low energy magnitude complies with the experimental observation of

the preference of staphylopine toward copper [17]. Such a mechanism suggests the release of copper to the *Staphylococcus* inner physiological medium, following the uptake of the complex by the bacterium. The case of Zn is very similar to that of Cu; however, other regions of the molecule are implicated in the LUMOs.

Figure 8 shows the NTO illustration of the excited-state TD-DFT calculations for STP–Zn, as shown for PSP–Zn (Figure 6). The similarity with the FMO in Figure 7 is even more pronounced than in PSP–Zn and equally points to an MLCT related mechanism.

Infrared Signature of the Complex

Figure 9 shows the calculated Infrared spectrum of STP–Cu. While main lines remain similar to the staphylopine in terms of their attribution (Figure 3, Table 1), new modes appear due to the presence of the copper ion. This is particularly the case for the so-called breathing mode at ~293 cm^{-1}. A movie showing this mode can be found in the Supplementary Materials. Nevertheless, other metal-related modes can be of significance upon identifying the spectroscopic fingerprint of the complexes. This can be relevant upon obtaining experimental spectra in further experiments.

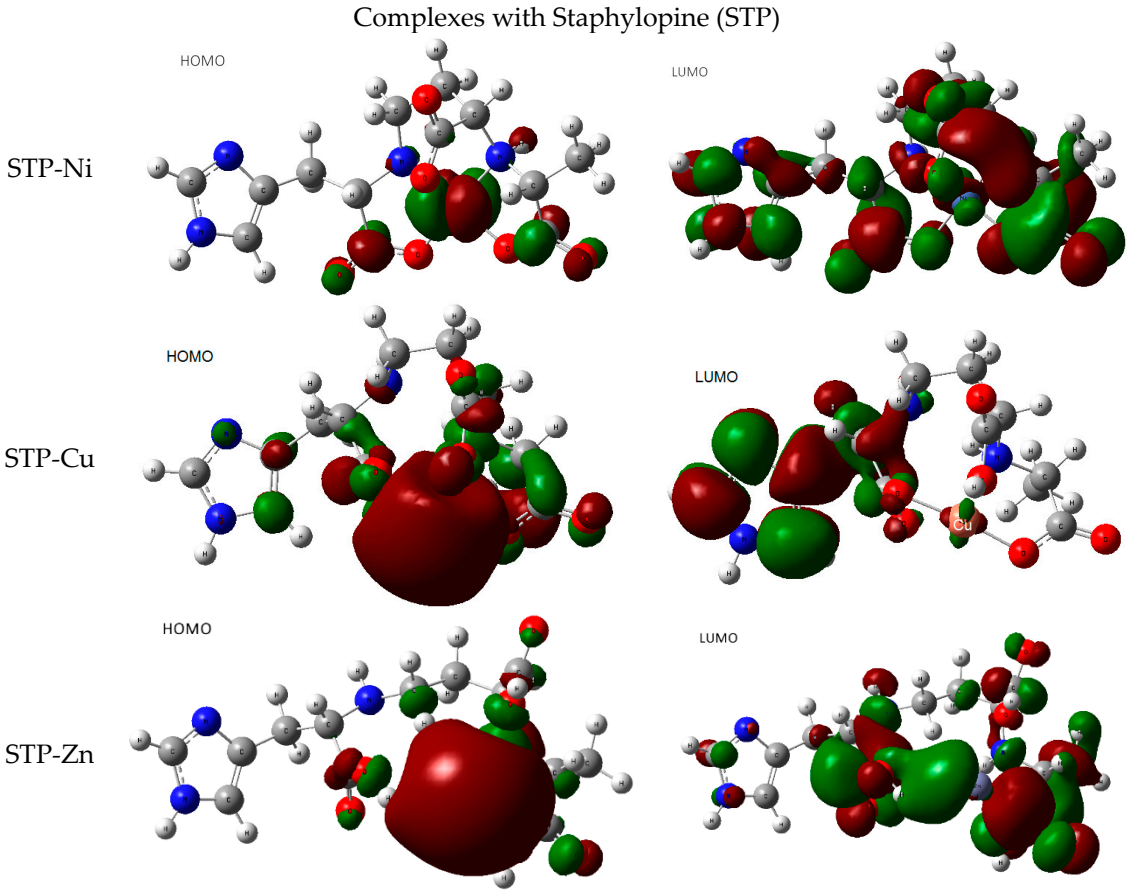

Figure 7. HOMOs and LUMOs of transition-metal complexes with STP (Ni, Cu, and Zn).

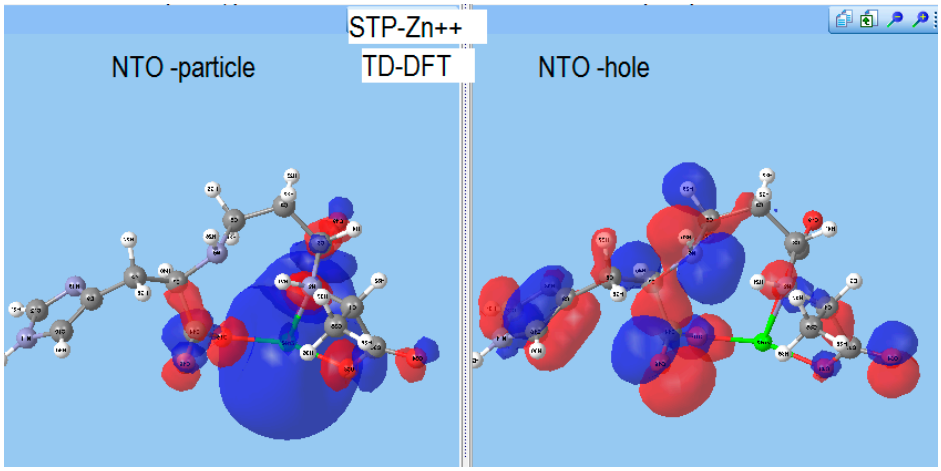

Figure 8. Natural transition (molecular) orbitals (NTOs) corresponding to FMOs of STP–Zn (cf. text).

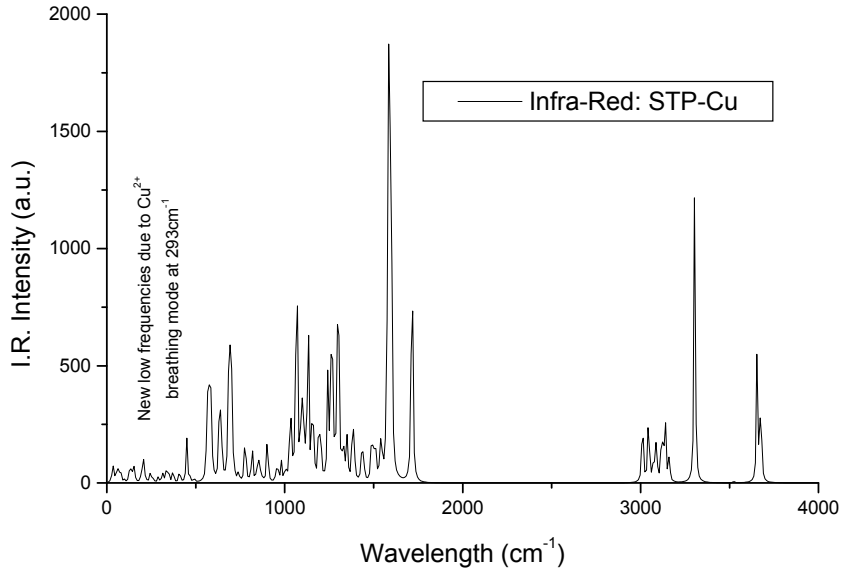

Figure 9. Calculated infrared spectrum of staphylopine chelated to divalent copper. Main lines remain similar to the metallophore infrared spectrum (Figure 3); however, new modes occur due to the presence of the copper ion, such as the "breathing mode" at ~293 cm^{-1}.

4. Concluding Notes and Future Perspectives

The aim of our investigation was to present a complementary view of a particularly relevant class of molecules in the field of bacterial pathology, i.e., transition-metal ion metallophores. Based on quantum chemical computations, further understanding of the active centers was provided for the following:

- two metallophores (pseudopaline and staphylopine);
- metal-chelated metallophores, mainly reporting on the charge transfers in frontier orbitals (HOMO to LUMO) where MLCT (metal-to-ligand charge transfer) mechanisms were identified, firstly inferred from FMOs, and further supported by NTOs from TD-DFT calculations.

The MLCT mechanism could be proposed as the basis of the delivery of the metallic ionic species to the bacterial medium. While making quantum-chemistry-based hypotheses, the authors are nevertheless aware that the mechanisms involved within the physiologic medium of the bacterium could be more complex.

The vibration spectroscopy signatures (infrared in this study) obtained with calculations should be of relevance once the corresponding metallophores and complexes are prepared at the laboratory

scale. Raman and UV–Vis signatures can also be obtained from quantum chemistry calculations, and these will help in further assessing prospective experimental works.

Our work here is only a first step toward a complete understanding of the domain of bacterial pathology, where experimental investigations are jointly required, especially for in vitro (laboratory) stepwise syntheses of metallophore molecules identified only within in vivo physiologic media, as well as computational investigations with other elaborate basis-set/functional frames.

Lastly, one should complementarily carry out multi-scale computations [33] along with further experimental findings, such as establishing crystal information files (CIFs) and more.

Supplementary Materials: The following are available online at http://www.mdpi.com/2079-3197/6/4/56/s1.

Author Contributions: Conceptualization, G.G.; Methodology, S.F.M.

Funding: This research received no external funding.

Acknowledgments: Massively parallel calculations with Gaussian 09 code were provided by the University of Bordeaux computer center MCIA. Discussions with Guillaume Chastanet of ICMCB (Institut de Chimie de la Matière Condensée; UMR-CNRS, University of Bordeaux) are gratefully acknowledged.

Conflicts of Interest: The authors declare no conflicts of interest.

References

1. Cohen, A.R. New advances in iron chelation therapy. *Am. Soc. Hematol.* **2006**, *2006*, 42–47. [CrossRef] [PubMed]
2. Finkenstedt, A.; Wolf, E.; Höfner, E.; Isasi Gasser, B.; Bösch, S.; Bakry, R.; Creus, M.; Kremser Ch Schocke, M.; Theur, M.; Moser, P.; et al. Hepatic but not brain iron is rapidly chelated by Deferasirox in aceruloplasminemia due to a novel gene mutation. *J. Hepatol.* **2010**, *53*, 1101–1107. [CrossRef] [PubMed]
3. Reniere, M.L.; Pishchany, G.; Skaar, E.P. *Iron Uptake and Homeostasis in Microorganisms*; Cornelis, P., Andrews, S.C., Eds.; Caister Academic Press: Norwich, UK, 2010; pp. 264–274.
4. Hood, M.I.; Skaar, E.P. Nutritional immunity: Transition metals at the pathogen–host interface. *Nat. Rev. Microbiol.* **2012**, *10*, 525–537. [CrossRef] [PubMed]
5. Budzikiewicz, A.G. Siderophores from bacteria and from fungi. In *Iron Uptake and Homeostasis in Microorganisms*; Corneis, P., Andrews, S.C., Eds.; Caister Academic Press: Norwich, UK, 2010; pp. 1–16.
6. Cornelissen, C.N.; Hollander, A. TonB-Dependent Transporters Expressed by Neisseria gonorrhoeae. *Front. Microbiol.* **2011**, *2*, 117. [CrossRef] [PubMed]
7. Minandri, F.; Imperi, F.; Frangipani, E.; Bonchi, C.; Visaggio, D.; Facchini, M.; Pasquali, P.; Bragonzi, A.; Visca, P. Role of Iron Uptake Systems in Pseudomonas aeruginosa Virulence and Airway Infection. *Infect. Immun.* **2016**, *84*, 2324–2335. [CrossRef] [PubMed]
8. Kim, H.J.; Graham, D.W.; DiSpirito, A.A.; Alterman, M.A.; Galeva, N.; Larive, C.K.; Asunskis, D.; Sherwood, P.M. Methanobactin, a copper-acquisition compound from methane-oxidizing bacteria. *Science* **2004**, *305*, 1612–1615. [CrossRef] [PubMed]
9. Dassama, L.M.K.; Kenney, G.E.; Ro, S.Y.; Zielazinski, E.L.; Rosenzweig, A.C. Methanobactin transport machinery. *Proc. Natl. Acad. Sci. USA* **2016**, *113*, 13027–13032. [CrossRef] [PubMed]
10. Si, M.; Zhao, C.; Burkinshaw, B.; Zhang, B.; Wei, D.; Wang, Y.; Dong, T.G.; Shen, X. Manganese scavenging and oxidative stress response mediated by type VI secretion system in *Burkholderia thailandensis*. *Proc. Natl. Acad. Sci. USA* **2017**, *114*, E2233–E2242. [CrossRef] [PubMed]
11. Cherrier, M.V.; Cavazza, C.; Bochot, C.; Lemaire, D.; Fontecilla-Camps, J.C. Structural characterization of a putative endogenous metal chelator in the periplasmic nickel transporter NikA. *Biochemistry (Mosc.)* **2008**, *47*, 9937–9943. [CrossRef] [PubMed]
12. Lebrette, H.; Borezée-Durant, E.; Martin, L.; Richaud, P.; Boeri Erba, E.; Cavazza, C. Novel insights into nickel import in Staphylococcus aureus: The positive role of free histidine and structural characterization of a new thiazolidine-type nickel chelator. *Metallomics* **2015**, *7*, 613–621. [CrossRef] [PubMed]
13. Shaik, M.M.; Cendron, L.; Salamina, M.; Ruzzene, M.; Zanotti, G. Helicobacter pylori periplasmic receptor CeuE (HP1561) modulates its nickel affinity via organic metallophores. *Mol. Microbiol.* **2014**, *91*, 724–735. [CrossRef] [PubMed]

14. Bobrov, A.G.; Kirillina, O.; Fetherston, J.D.; Miller, M.C.; Burlison, J.A.; Perry, R.D. The Yersinia pestis Siderophore, Yersiniabactin, and the ZnuABC system both contribute to Zinc acquisition and the development of lethal septicemic plague in mice. *Mol. Microbiol.* **2014**, *93*, 759–775. [CrossRef] [PubMed]
15. Bobrov, A.G.; Kirillina, O.; Fosso, M.Y.; Fetherston, J.D.; Miller, M.C.; VanCleave, T.T.; Burlison, J.A.; Arnold, W.K.; Lawrenz, M.B.; Garneau-Tsodikova, S.; et al. Zinc transporters YbtX and ZnuABC are required for the virulence of Yersinia pestis in bubonic and pneumonic plague in mice. *Met. Integr. Biomet. Sci.* **2017**, *9*, 757–772. [CrossRef] [PubMed]
16. Kallifidas, D.; Pascoe, B.; Owen, G.A.; Strain-Damerell, C.M.; Hong, H.J.; Paget, M.S. The zinc-responsive regulator Zur controls expression of the coelibactin gene cluster in *Streptomyces coelicolor*. *J. Bacteriol.* **2010**, *192*, 608–611. [CrossRef] [PubMed]
17. Ghssein, G.; Brutesco, C.; Ouerdane, L.; Fojcik, C.; Izaute, A.; Wang, S.; Hajjar, C.; Lobinski, R.; Lemaire, D.; Richaud, P.; et al. Biosynthesis of a broad-spectrum nicotianamine-like metallophore in *Staphylococcus aureus*. *Science* **2016**, *352*, 1105–1109. [CrossRef] [PubMed]
18. Lhospice, S.; Gomez, N.O.; Ouerdane, L.; Brutesco, C.; Ghssein, G.; Hajjar, C.; Liratni, A.; Wang, S.; Richaud, P.; Bleves, S.; et al. Pseudomonas aeruginosa zincuptake in chelating environmentis primarily mediated by the metallophore pseudopaline. *Sci. Rep.* **2017**, *7*, 17123. [CrossRef] [PubMed]
19. Zhang, J.; Wang, S.; Bai, Y.; Guo, Q.; Zhou, J.; Lei, X. Total Syntheses of Natural Metallophores Staphylopine and Aspergillomarasmine A. *J. Org. Chem.* **2017**, *82*, 13643–13648. [CrossRef] [PubMed]
20. Fukui, K.; Yonezawa, T.; Shingu, H. A Molecular Orbital Theory of Reactivity in Aromatic Hydrocarbons. *J. Chem. Phys.* **1952**, *20*, 722. [CrossRef]
21. Atkins, P.W.; Friedman, R. *Molecular Quantum Mechanics*, 4th ed.; Oxford University Press: New York, NY, USA, 2005; ISBN 978-0-19-927498-7.
22. Hohenberg, P.; Kohn, W. Inhomogeneous Electron Gas. *Phys. Rev. B* **1964**, *136*, 864. [CrossRef]
23. Kohn, W.; Sham, L.J. Self-Consistent Equations Including Exchange and Correlation Effects. *Phys. Rev. A* **1965**, *140*, 1133. [CrossRef]
24. Ceperley, D.M.; Alder, B.J. Ground State of the Electron Gas by a Stochastic Method. *Phys. Rev. Lett.* **1980**, *45*, 566–569. [CrossRef]
25. Perdew, J.; Burke, K.; Ernzerhof, M. Generalized Gradient Approximation Made Simple. *Phys. Rev. Lett.* **1996**, *77*, 3865–3868. [CrossRef] [PubMed]
26. Reiher, M.; Salomonn, O.; Hess, B.A. Reparameterization of hybrid functionals based on energy differences of states of different multiplicity. *Theor. Chem. Acc.* **2001**, *107*, 48–55. [CrossRef]
27. Ditchfield, R.; Hehre, W.J.; Pople, J.A. Self-Consistent Molecular-Orbital Methods. *J. Chem. Phys.* **1971**, *54*, 724. [CrossRef]
28. *Gaussian09, Revision D.01*; Gaussian, Inc.: Wallingford, CT, USA, 2009.
29. Cossi, M.; Barone, V.; Cammi, R.; Tomasi, J. Ab initio study of solvated molecules: A new implementation of the polarizable continuum model. *Chem. Phys. Lett.* **1996**, *255*, 327–335. [CrossRef]
30. Martin, R.L. Natural transition orbitals. *J. Chem. Phys.* **2003**, *118*, 4775. [CrossRef]
31. Zerdane, S.; Collet, E.; Dong, X.; Matar, S.F.; Wang, H.F.; Desplanches, C.; Chastanet, G.; Chollet, M.; Glownia, J.M.; Lemke, H.; et al. Electronic and Structural Dynamics During the Switching of the Photomagnetic Complex [Fe(L222N5)(CN)2]. *Chem. Eur. J.* **2018**, *24*, 5064. [CrossRef] [PubMed]
32. Song, L.; Zhang, Y.; Chen, W.; Gu, T.; Zhang, S.-Y.; Ji, Q. Mechanistic insights into staphylopine-mediated metal acquisition. *Proc. Natl. Acad. Sci. USA* **2018**, *115*, 3942–3947. [CrossRef] [PubMed]
33. Matar, S.F.; Guionneau, P.; Chastanet, G. Multiscale Experimental and Theoretical Investigations of Spin Crossover FeII Complexes: Examples of $[Fe(phen)_2(NCS)_2]$ and $[Fe(PM\text{-}BiA)_2(NCS)_2]$. *Int. J. Mol. Sci.* **2015**, *16*, 4007–4027. [CrossRef] [PubMed]